Am J Physiol Lung Cell Mol Physiol 290: L1247–L1259, 2006.
First published January 20, 2006; doi:10.1152/ajplung.00450.2005.

Manganese and iron transport across pulmonary epithelium

Elizabeth A. Heilig,[1,2] Khristy J. Thompson,[1] Ramon M. Molina,[2] Alexander R. Ivanov,[3] Joseph D. Brain,[2] and Marianne Wessling-Resnick[1]

[1]*Department of Genetics and Complex Diseases,* [2]*Department of Environmental Health,* [3]*Harvard NIEHS Center for Environmental Health Proteomics Facility, Harvard School of Public Health, Boston, Massachusetts*

Submitted 27 October 2005; accepted in final form 13 January 2006

Heilig, Elizabeth A., Khristy J. Thompson, Ramon M. Molina, Alexander R. Ivanov, Joseph D. Brain, and Marianne Wessling-Resnick. Manganese and iron transport across pulmonary epithelium. *Am J Physiol Lung Cell Mol Physiol* 290: L1247–L1259, 2006. First published January 20, 2006; doi:10.1152/ajplung.00450.2005.—Pathways mediating pulmonary metal uptake remain unknown. Because absorption of iron and manganese could involve similar mechanisms, transferrin (Tf) and transferrin receptor (TfR) expression in rat lungs was examined. Tf mRNA was detected in bronchial epithelium, type II alveolar cells, macrophages, and bronchus-associated lymphoid tissue (BALT). Tf protein levels in lung and bronchoalveolar lavage fluid did not change in iron deficiency despite increased plasma levels, suggesting that lung Tf concentrations are regulated by local synthesis in a manner independent of body iron status. Iron oxide exposure upregulated Tf mRNA in bronchial and alveolar epithelium, macrophages, and BALT, but protein was not significantly increased. In contrast, TfR mRNA and protein were both upregulated by iron deficiency. To examine potential interactions with lung Tf, rats were intratracheally instilled with ^{54}Mn or ^{59}Fe. Unlike ^{59}Fe, interactions between ^{54}Mn and Tf in lung fluid were not detected. Absorption of intratracheally instilled ^{54}Mn from the lungs to the blood was unimpaired in Belgrade rats homozygous for the functionally defective G185R allele of divalent metal transporter-1, indicating that this transporter is also not involved in pulmonary manganese absorption. Pharmacological studies of ^{54}Mn uptake by A549 cells suggest that metal uptake by type II alveolar epithelial cells is associated with activities of both L-type Ca^{2+} channels and TRPM7, a member of the transient receptor potential melastatin subfamily. These results demonstrate that iron and manganese are absorbed by the pulmonary epithelium through different pathways and reveal the potential role for nonselective calcium channels in lung metal clearance.

transferrin; bronchoalveolar lavage fluid; macrophages

INHALATION IS AN IMPORTANT route of exposure to toxic trace metals. Particulate matter in urban environments typically contains multiple transition metals, including Fe, Mn, Cu, Ni, Zn, Co, V, Cr, and Ti (41). Metals in particulate matter may contribute to inflammation, exacerbating preexisting conditions such as asthma and chronic obstructive pulmonary disease (14, 23). Once inhaled particles are dissolved, metals can enter the bloodstream and be taken up by other tissues, in some cases resulting in toxicity in other organs. In particular, chronic inhalation exposure to high levels of manganese can induce pulmonary effects in animals (20) and humans (44) and can cause neurotoxicity, or manganism, an extrapyramidal disorder with symptoms resembling those of Parkinson's disease (3, 15). Sources of exposure to manganese include welding fume, dust produced in manganese ore processing plants, manganese mining, and certain pesticides (3). Manganese is also released into the air by combustion of gasoline containing the additive manganese methylcyclopentadienyl tricarbonyl (62).

The mechanisms involved in metal uptake by pulmonary epithelial cells, and transport of trace metals across the air-blood barrier, are not fully understood. For manganese and iron, understanding the interplay between regulation of transporters by iron status, and competition (or lack thereof) for different transport mechanisms, would be of significant benefit in risk assessment for mixtures of iron and manganese particles, as found in welding fume.

Divalent metal transporter-1 (DMT1/Nramp2/SLC11A2) is expressed by pulmonary epithelial cells and appears to play an important role in regulation of iron homeostasis in the lungs. Belgrade rats, which possess a naturally occurring point mutation in DMT1 (G185R) that results in protein misfolding and degradation, exhibit reduced clearance of iron and vanadium from the lungs after instillation with residual oil fly ash (ROFA) (25). DMT1 expression is upregulated in bronchial epithelium of rats exposed to ferric ammonium citrate, supporting a role in detoxification (56). DMT1 can transport several other divalent metal ions in addition to iron, including manganese (26).

The iron-binding proteins transferrin (Tf), ferritin, and lactoferrin are also synthesized by pulmonary epithelial cells. These soluble iron-binding factors are found in pulmonary fluid and are thought to contribute to regulation of free iron levels in the lungs and the prevention of oxidative damage (24, 39, 51, 60). The ferroxidase ceruloplasmin is also present in pulmonary fluid and could potentially oxidize Fe^{2+} to Fe^{3+}, thereby limiting oxidative damage caused by highly reactive ferrous iron and promoting interaction of ferric iron with Tf (39).

Tf not only binds Fe^{3+}, but can also bind Mn^{3+}, albeit with lower affinity (2). Receptor-mediated endocytosis of Tf by transferrin receptor (TfR) expressed on the apical surface of pulmonary epithelial cells therefore could be an important mechanism for clearance of iron, manganese, and other metals from airway and alveolar fluid. DMT1 also plays a key role in TfR-mediated iron uptake as the transporter of iron released from Tf in the endocytic vesicle into the cytoplasm and would be envisioned to have an analogous role in uptake of Mn-Tf via this pathway. As for iron, the speciation of manganese would be an important determinant for transport mediated by DMT1 across the plasma membrane (Mn^{2+}) or for uptake by TfR-mediated endocytosis of Tf-bound metal (Mn^{3+}). Whether

Address for reprint requests and other correspondence: M. Wessling-Resnick, Dept. of Genetics and Complex Diseases, Harvard School of Public Health, 665 Huntington Ave., Boston, MA 02115 (e-mail: wessling@hsph.harvard.edu).

The costs of publication of this article were defrayed in part by the payment of page charges. The article must therefore be hereby marked "*advertisement*" in accordance with 18 U.S.C. Section 1734 solely to indicate this fact.

Mn^{2+} would be converted to Mn^{3+} by lung fluid oxidases (e.g., ceruloplasmin) remains unknown.

In addition to the Tf/TfR/DMT1-mediated pathway for metal uptake, there is mounting evidence that nonselective calcium channels transport divalent iron and manganese. Fe^{2+} and Mn^{2+} uptake by cardiomyocytes in vitro (52) and uptake of Fe^{2+} by in situ-perfused heart (33) are both partially blocked by inhibitors of L-type voltage-gated channels (LVGCs) and increased by LVGC activators. Mn^{2+} uptake by liver was found to be sensitive to the LVGC inhibitor nifedipine (12). Similar analysis of isolated blood-brain-barrier-derived cells, and in situ brain perfusion assays, has demonstrated sensitivity of Mn^{2+} uptake to store-operated calcium channel (SOC) inhibitors and activators (17). Several members of the transient receptor potential (TRP) family of receptor- and store-operated calcium channels have also been implicated in transport of multiple divalent metal ions. For example, use of Mn^{2+} as a proxy for Ca^{2+} in patch-clamp experiments has demonstrated that TRPC1, TRPC3, TRPC4, TRPC5, and TRPC6 are permeable to manganese ions (9, 29).

Previously, we observed that the in vivo pharmacokinetics for intratracheally instilled ^{54}Mn and ^{59}Fe were remarkably different, suggesting that these metals cross the pulmonary epithelium through different molecular mechanisms (28). Here, we further examine pathways for transport of these metals by pulmonary epithelial cells. Our results demonstrate that after instillation of soluble divalent forms, iron and manganese appear to be cleared from the lungs by distinct mechanisms. Evidence from in vitro studies of ^{54}Mn transport by A549 type II alveolar epithelial cells suggests that nonselective calcium channels may play an important role in uptake of manganese ions by pulmonary epithelial cells.

MATERIALS AND METHODS

Animal care and diets. Animal protocols for this study were approved by the Harvard Medical Area Animal Care and Use Committee of Harvard University. Male CD/HSD rats (21 days) were purchased from Harlan Sprague Dawley (Indianapolis, IN). Rats were maintained on a 12:12-h light-dark cycle and were given food and water ad libitum. To induce iron deficiency, rats were fed a low-iron diet containing 20–25 ppm Fe for 3 wk (Purina test diet no. 7444; PharmaServ, Framingham, MA). Age-matched control rats were fed a standard diet containing ~200 ppm Fe (Purina diet no. 5053). Iron deficiency was confirmed by measurement of hematocrit as described previously (28); hematocrits of Fe-deficient rats were significantly lower than in control animals (27.7 vs. 44.8%, respectively). For iron oxide particle exposure, rats were intratracheally instilled with a suspension of iron oxide particles (mass median aerodynamic diameter of 0.68 μm) generated by the combustion of iron pentacarbonyl vapor (55). Rats were placed on a slanted platform, supported by an elastic band placed under the upper incisors. Iron oxide particle suspension in sterile PBS was delivered to the lungs via a blunt 18-gauge needle inserted between the laryngeal folds and into the trachea. Transillumination of the larynx was provided by a microscope lamp shining on the neck (8). Rats were instilled with 7.5 mg iron oxide·kg^{-1}·day^{-1} every 3 days for a total of five instillations in 2 wk and were humanely killed 3 wk after commencement of instillations. Lung nonheme iron levels were significantly elevated in these animals as previously determined (7).

To study metal binding by lung fluid proteins, $^{54}MnCl_2$ and $^{59}FeCl_3$ were purchased from Perkin Elmer/New England Nuclear (Boston, MA). ^{59}Fe was diluted with 1:20 molar excess of ascorbic acid immediately before the experiment. Radioisotopes were further diluted to 13.3 μCi ^{59}Fe/ml and 14.7 μCi ^{54}Mn/ml in sterile PBS immediately before instillation. To deliver radioisotope to the lungs, rats were anesthetized with vaporized halothane (Halocarbons Lab, North Augusta, SC) and intratracheally instilled as described above with a delivery volume of 1.5 ml per kilogram of body weight. Ten minutes or 1 h postinstillation, rats were anesthetized with pentobarbital sodium and killed by exsanguination. The trachea was then cannulated and the lungs were lavaged once with 3 ml of sterile PBS. Bronchoalveolar lavage (BAL) samples were centrifuged at 3,000 *g* for 10 min at 4°C to remove cells and supernatants were immediately processed for fast protein liquid chromatography (FPLC) studies or stored at −80°C for Western blot analysis.

A Belgrade rat colony was established with animals obtained from Dr. M. Garrick (SUNY-Buffalo). Mating pairs of female *+/b* and male *b/b* rats were maintained on an iron-supplemented diet containing 500 ppm ferrous iron (TD02385, Harlan Teklad, Madison, WI). Female *+/b* rats were fed the iron-supplemented diet throughout pregnancy. At postnatal *day 6*, litters were cross-fostered onto F344 Fischer dams (Harlan Sprague Dawley) fed a standard diet containing 200 ppm iron (Purina diet no. 5053, PharmaServ). On weaning, *b/b* and *+/b* rats were fed the iron-supplemented diet (500 ppm). Belgrade (*b/b*) pups were identified at birth by pale, anemic features and genotype was verified by PCR as described by Fleming et al. (21).

To determine the pharmacokinetics of manganese absorption after intratracheal instillation, *b/b* and *+/b* rats were anesthetized with vaporized halothane. $^{54}MnCl_2$ diluted to 10 μCi/ml in PBS was administered by intratracheal instillation as described above (final delivery volume of 1.5 ml/kg body wt). Blood samples were collected from the tail vein at 5, 15, and 30 min and at 1, 2, and 4 h postinstillation. Rats were killed 4 h postinstillation and brain, heart, liver, lung, bone marrow, muscle, kidney, stomach, small intestine and large intestine were collected for measurement of associated ^{54}Mn. All tissue and blood samples were weighed and radioactivity was measured in a Packard gamma counter (Cobra Quantum, Packard Instrument, IL), and ^{54}Mn level was calculated as a percentage of the instilled dose.

In situ hybridization. After death, the tracheas of control and iron-deficient rats were cannulated with a blunt 18-gauge needle and syringe containing optimum cutting temperature (OCT) compound (Sakura Finetek USA, Torrance, CA) prewarmed to 37°C. Lungs were filled with OCT, cut laterally into sections, mounted in OCT, snap-frozen in 2-methylbutane chilled on dry ice, and stored at −80°C. Ten-micrometer-thick sections were cut on a cryotome and stored at −20°C until processed. Digoxigenin-labeled sense and antisense cRNA probes were transcribed from a full-length rat Tf cDNA (generously supplied by Dr. S. Hisayasu, Tokyo, Japan) or a 594-bp rat TfR EST (Resgen/Invitrogen, Carlsbad, CA), flanked by T7 and T3 promoter sites. Transcripts were shortened to an average length of 200−400 bp by alkali hydrolysis. Sections were incubated with sense or antisense probe (~200 ng/ml) in hybridization buffer (50% formamide, 5× SSC, 2% blocking reagent, 0.02% SDS, 0.1% *N*-lauryl-sarcosine). Hybridized probes were detected using anti-digoxigenin-alkaline phosphatase-coupled Fab fragments and bromo-4-chloro-3-indoxyl-phosphate and nitro blue tetrazolium as a substrate. Sections were incubated in substrate solution for 42 h, rinsed in TE buffer (10 mM Tris and 1 mM EDTA, pH 8.0), and mounted in 50% PBS-glycerol.

Detection of proteins by Western blotting. Snap-frozen lung tissue from control, Fe-deficient, or Fe oxide-exposed rats was homogenized on ice in 20 mM HEPES, pH 7.4, 100 mM KCl, 85 mM sucrose, 20 μM EGTA, 1% Triton X-100, with Complete Mini protease inhibitor cocktail (Roche, Indianapolis, IN) added. Homogenates were incubated at 4°C with rotation for 45 min and then clarified by centrifugation for 10 min at 12,000 *g*. Protein concentration in supernatants was measured by Bradford assay (6). Samples of 120 μg lung protein or 20 μg BAL protein were electrophoresed on 10 or 7% SDS-polyacrylamide gels, respectively, and transferred to nitrocellulose for

immunoblotting. Membranes were blocked with 5% nonfat dry milk in TBST (50 mM Tris, 150 mM NaCl, 0.1% Tween 20, pH 7.4) for 1 h at room temperature, then incubated with mouse anti-human TfR (1:1,000; Zymed, San Francisco, CA), rabbit anti-human Tf (1:2,000, Rockland), sheep anti-human ferritin (1:1,000, The Binding Site, Birmingham, UK) or mouse anti-α-tubulin (1:10,000, Sigma, St. Louis, MO) overnight at 4°C. Secondary horseradish peroxidase-labeled goat anti-mouse IgG (1:40,000, Pierce, Rockford, IL) or donkey anti-rabbit IgG (1:40,000, Pierce) was used to detect immunoreactivity by enhanced chemiluminescence using SuperSignal West Pico Reagent (Pierce). Intensity of bands was quantified with Bio-Rad QuantityOne software.

FPLC fractionation of BAL fluid. After intratracheal instillation of ^{54}Mn or ^{59}Fe as described above, BAL supernatant was centrifuged at 12,000 *g* for 15 min to remove insoluble material and debris. Two milliliters were then dialyzed (Spectra/Por, MWCO 12,000–14,000; Spectrum Laboratories, Rancho Dominguez, CA) against FPLC *buffer A* (25 mM Tris, pH 8.5) for 4–6 h at 4°C to lower salt concentration. Samples were loaded on a MonoQ anion-exchange column and proteins were eluted with a two-step linear salt gradient (40 ml of 0–0.5 M NaCl, followed by 20 ml 0.5–1.00 M NaCl). Radioactivity in 1-ml fractions from FPLC, along with cpm in lungs, BAL cell pellet, and BAL (pre- and postdialysis) was measured by gamma counting.

For FPLC fractionation of ^{54}Mn-Tf, a 100-μl solution containing 12.5 μM human apo-Tf (Sigma), 125 μM $MnCl_2$, and 125 nM $^{54}MnCl_2$ (0.3 μCi) in 15 mM $NaHCO_3$ (pH 8.0) was incubated at 37°C for 5 h. The binding of manganese to Tf was confirmed by measuring the absorbance ratio at 300 nm/280 nm (16), and ^{54}Mn-Tf was subsequently dialyzed (molecular weight cutoff 12,000–14,000) against FPLC *buffer A* for 12–16 h at 4°C. ^{54}Mn-Tf was fractionated by FPLC on a MonoQ column exactly as described above.

Protein fractions were precipitated overnight at 4°C (25% trichloroacetic acid, 0.02% casamino acids), washed twice with ice-cold acetic acid, and resuspended by boiling for 10 min in 1× Laemmli buffer containing 1% β-mercaptoethanol. Fractions were electrophoresed on 5–20% SDS-polyacrylamide gels and proteins were visualized by either Coomassie blue or silver staining. Bands of interest were excised and digested overnight at 37°C in 50 mM NH_4HCO_3 containing 10–20 μg/ml trypsin. Tryptic peptides were extracted with one change of 20 mM NH_4HCO_3, two changes of 5% formic acid in 50% acetonitrile, and one change of 5% formic acid in 50% isopropanol at room temperature. For identification of proteins by nano-liquid chromatography (LC) electrospray ionization tandem mass spectrometry, digests were injected onto a C18 solid-phase extraction column for desalting, eluted onto and separated on a nano-LC column with a linear gradient of acetonitrile in 0.1% formic acid, and the eluent was introduced into a LCQ Deca XP Plus mass spectrometer by nanoelectrospray. A full MS scan between 400 and 1,800 m/z was performed, followed by five MS/MS scans for the five most intense ions from the MS scan acquired in data-dependent MS/MS scanning experiments. Data files were converted to .dta files using Bioworks 3.2 software (ThermoElectron) and submitted to the database search against a composite [forward and reversed (40)] protein sequence database derived from NCBI rat database on a Sorcerer search station (Sage-N, Thermo Electron, Philadelphia, PA) using SEQUEST algorithm. SEQUEST output (.out files) was analyzed using DTASelect software (provided by Dr. J. Yates, Scripps Research Institute).

^{54}Mn and ^{55}Fe uptake assays. A549 cells (ATCC no. CCL-185; kindly provided by Dr. D. Tschumperlin, Harvard School of Public Health) were maintained in DMEM/F12 (1:1) media (Mediatech, Herndon, VA) supplemented with 10% fetal bovine serum (Gemini Bio Products, Woodland, CA) and seeded at a density of 3.6×10^5 cells per well in 6-well plates, or 1.6×10^5 cells per well in 12-well plates, 24 h before uptake assays. Cells were subconfluent (70–80%) at time of assays. Cells were washed 3× with HeBS (20 mM HEPES, 137 mM NaCl, 0.5 mM Na_2HPO_4, 0.5 mM KCl, pH 7.4) and then incubated with 1–2 μCi $^{54}MnCl_2$ (Perkin Elmer/New England Nuclear) in HeBS with drugs or vehicle for 4 min at 37°C unless otherwise indicated. After being washed 3× with HeBS, cells were incubated with 100 mM $MnCl_2$ in HeBS for 1 h at 4°C to eliminate nonspecific binding of ^{54}Mn. Cells were then washed 3× in HeBS and lysed in 600 μl of solubilization buffer (0.02 M NaOH, 0.1% Triton X-100). Simultaneous control assays were performed at 4°C for all treatments. For assays with ^{55}Fe, a stock solution of ^{55}Fe-nitrilotriacetic acid (1:4) was diluted with a 1:50 molar ratio of freshly made ascorbic acid immediately before each assay, then diluted further in HeBS uptake buffer at indicated pH. Radioactivity of lysates was measured in a gamma (^{54}Mn) or beta (^{55}Fe) counter, and protein concentration was determined by Bradford assay. Specific uptake was taken as the difference between uptake measured at 37 and 4°C and was calculated as picomole Mn per microgram of protein. $MgCl_2$, $NiCl_2$, and $CaCl_2$ stocks were 0.1–1.0 M in H_2O. $FeCl_3$ was dissolved in water and mixed with a 1:50 molar excess of ascorbic acid immediately before use. Drug stocks were prepared as follows: verapamil, 10 mM in H_2O; amiloride, 10 mM in DMSO; thapsigargin, 3 mM in DMSO; nifedipine, 10 mM in ethanol; BAY K 8644, 0.1 mM in ethanol; 2-aminoethoxydiphenyl borate (2-APB), 10 mM in DMSO; and oleylacetylglycerol (OAG), 20 mM in DMSO.

RT-PCR. RNA was isolated from subconfluent A549 cells with RNA-Bee (Tel-Test, Friendswood, TX) following the manufacturer's instructions. RNA was treated with DNase I (Promega, Madison, WI) to remove genomic DNA, extracted with phenol-chloroform-isoamyl alcohol (25:24:1) mixture, precipitated, resuspended in diethyl pyrocarbonate-treated water, and quantified by UV spectrophotometry. cDNA was synthesized from 2 μg RNA in reactions containing 1× Moloney murine leukemia virus-reverse transcriptase (MMLV-RT) buffer, 0.5 mM dNTP mix, 25 μg/ml oligo(dT)15 primer, 5 mM $MgCl_2$, 10 mM dithiothreitol, 1 U of RNasin, and 200 U of MMLV-RT enzyme (Promega). MMLV-RT enzyme was ommitted for RT-control reactions. Amplification reactions were carried out with 1 μl of cDNA in 1× PCR buffer (10 mM Tris·HCl, pH 9.0, 50 mM KCl, 2.0 mM $MgCl_2$; Promega). Sequences of primers for TRPC1–6 were previously published elsewhere (53). Sequences of other primers used are as follows: TRPC7 forward, 5′-CTGCCAGCCAACGAGAGT-3′; TRPC7 reverse, 5′-TCATCAAAGTAAGACAGCCAGAGT-3′; TRPM7 forward, 5′-TCCAGCACAGTTAAAAGGTCAATA-3′; TRPM7 reverse, 5′-GTCTTCAGTTCAGGCTTCTCATAC-3′; LVGC (α-subunit) forward, 5′-AGAATCTGGGCAGAGTATGAC-3′; and LVGC reverse, 5′-CAGGAACGTGGCGTAGAACTT-3′.

Fifteen microliters of each reaction were separated on a 1.2% agarose gel containing ethidium bromide, and band intensity was quantified with QuantityOne software (Bio-Rad, Hercules, CA).

Statistical analysis. All values are means ± SE. Comparisons of protein expression measured by Western blotting and A549 cell metal uptake assays were evaluated by unpaired Student's *t*-test. Characteristics of the pharmacokinetics of manganese transport and tissue distribution of ^{54}Mn were evaluated by multivariate ANOVA (MANOVA) using the general linear model procedure (SAS statistical analysis software; SAS Institute, Cary, NC). Statistical significance was based on an α level of 0.05.

RESULTS

Expression of transferrin in lungs. Expression and iron-responsive regulation of Tf and TfR were examined by in situ hybridization and Western blot analysis of lung tissue from control, iron-deficient, and iron oxide-exposed rats. In control animals, Tf mRNA was detected in type II alveolar epithelial cells, alveolar macrophages, bronchial epithelium, and in localized regions of bronchus-associated lymphoid tissue (BALT; Fig. 1, *A* and *D*). Tf mRNA expression in iron-deficient rats exhibited the same localization pattern and stain-

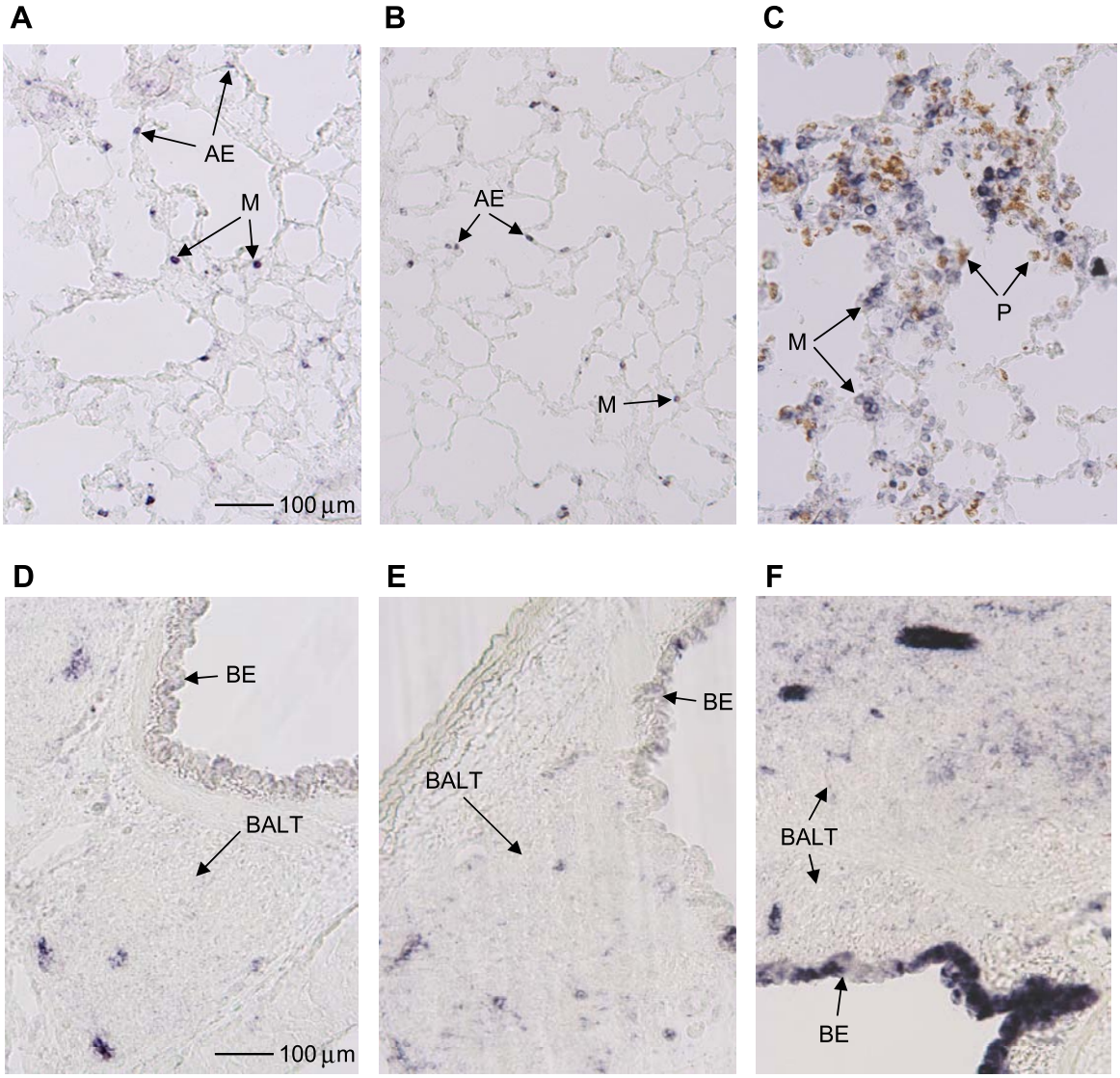

Fig. 1. In situ hybridization detecting lung transferrin (Tf) mRNA expression. Ten-micrometer-thick cryosections of lungs from control (*A*, *D*), iron-deficient (*B*, *E*), and iron oxide-exposed (*C*, *F*) rats embedded in optimum cutting temperature (OCT) were hybridized with digoxigenin-labeled sense and antisense Tf probes as described under MATERIALS AND METHODS. Tf mRNA is detected by an alkaline phosphatase-coupled reaction (bluish-purple staining) and iron oxide particles appear brown (*C*, *F*). AE, alveolar epithelial cell; M, macrophage; P, particle-containing macrophage; BALT, bronchus-associated lymphoid tissue; BE, bronchial epithelium. Magnification ×10.

ing intensity as in controls (Fig. 1, *B* and *E*). In iron oxide-exposed lung, staining for Tf mRNA was greater in BALT and bronchial epithelium than in control lung (Fig. 1*F*) and appeared more intense in alveolar epithelial cells and macrophages in regions where iron particles were deposited (Fig. 1*C*).

Western blot analysis indicated that Tf protein levels were not significantly altered in lung tissue from either iron-deficient or iron oxide-exposed rats. To examine whether Tf levels in pulmonary fluid change in iron deficiency, protein levels in BAL fluid from control and iron-deficient rats were quantified by Western blotting. While plasma levels were significantly elevated in iron-deficient rats as expected, the level of Tf in BAL was not significantly different from controls (Figs. 2 and 3). Because circulating plasma Tf levels are significantly elevated in dietary iron deficiency (5), the apparent lack of change in BAL Tf levels in iron-deficient animals suggests that the concentration of this protein in pulmonary fluid reflects synthesis by the lungs (60) in a manner that is independent of body iron status.

Expression of transferrin receptor in lungs. TfR mRNA was detected only in BALT and bronchial epithelium of control rats (Fig. 4, *A* and *D*). In iron-deficient rats, similar staining intensity was observed in BALT and bronchial epithelium (Fig. 4*E*), while upregulation of TfR message was observed in type II alveolar epithelial cells (Fig. 4*B*). In contrast, staining in iron oxide-exposed rats was significantly stronger in BALT and bronchial epithelium (Fig. 4*F*) and was also increased in alveolar epithelium and in macrophages in areas of iron oxide particle deposition (Fig. 4*C*).

Western blot analysis to examine iron-responsive changes in lung TfR indicated that protein levels were significantly increased in iron-deficient rat lung (Fig. 2). In contrast to mRNA levels, however, the level of TfR protein did not change in iron

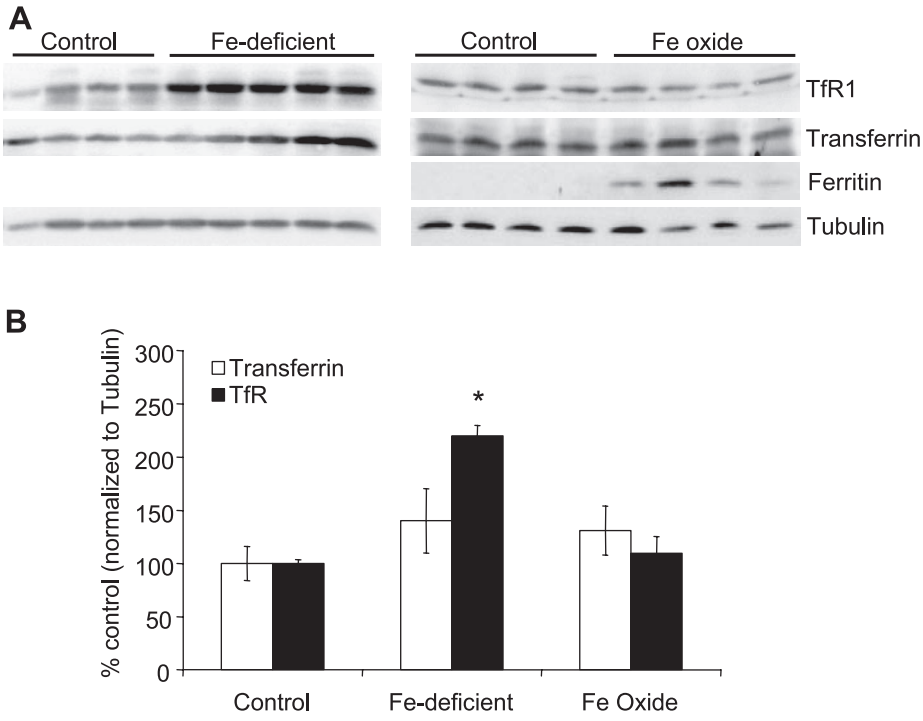

Fig. 2. Transferrin receptor (TfR), Tf, and ferritin protein levels in control, Fe-deficient, and Fe oxide-exposed rat lung. *A*: Western blot analysis was performed as described under MATERIALS AND METHODS. Lanes contain samples from individual animals. Separate experiments were conducted for Fe-deficient and Fe oxide-exposed groups, with age-matched controls. Note that ferritin levels were below limit of detection in control and Fe-deficient lung. *B*: Tf and TfR protein expression levels in *A* were quantified (QuantityOne imaging software, Bio-Rad). Values are expressed as % control and normalized to α-tubulin expression level. *$P < 0.0005$ ($n = 4$ to 5; means ± SE).

oxide-exposed lung. Ferritin levels were significantly higher in iron oxide-exposed lung, confirming increased tissue iron levels.

Interaction of ^{54}Mn and ^{59}Fe with proteins in BAL fluid. To determine whether soluble manganese or iron introduced into the lungs interacts with Tf in pulmonary fluid, rats were intratracheally instilled with ^{54}Mn or ^{59}Fe and lavage fluid was collected 10 min postinstillation. Although the levels associated with lung tissue were comparable for ^{54}Mn and ^{59}Fe (~55% instilled dose), significant differences were observed in the distribution of the radioisotopes in BAL fluid (Table 1). Only ~14% of instilled ^{54}Mn remained in BAL fluid after 10 min of which 1% was found to be associated with protein (as determined by dialysis). In contrast, 27% of instilled ^{59}Fe was found in BAL, of which 22% was bound to protein. To examine the association of the radioisotopes with Tf in lung fluid, in vivo-radiolabeled BAL samples were fractionated by anion-exchange chromatography using fast-performance liquid chromatography. The two major chromatographic peaks were identified as Tf (*fraction 17*) and albumin (*fractions 26-27*) by Western blotting (data not shown). After dialysis of BAL fluid, ^{59}Fe was found predominantly in *fraction 17* containing the peak for Tf (Fig. 5*A*). In contrast, ^{54}Mn was detected only in *fraction 15* (Fig. 5*B*). Fractionation of BAL fluid collected 1 h after instillation of ^{54}Mn demonstrated that only trace amounts of ^{54}Mn are associated with protein in pulmonary fluid after

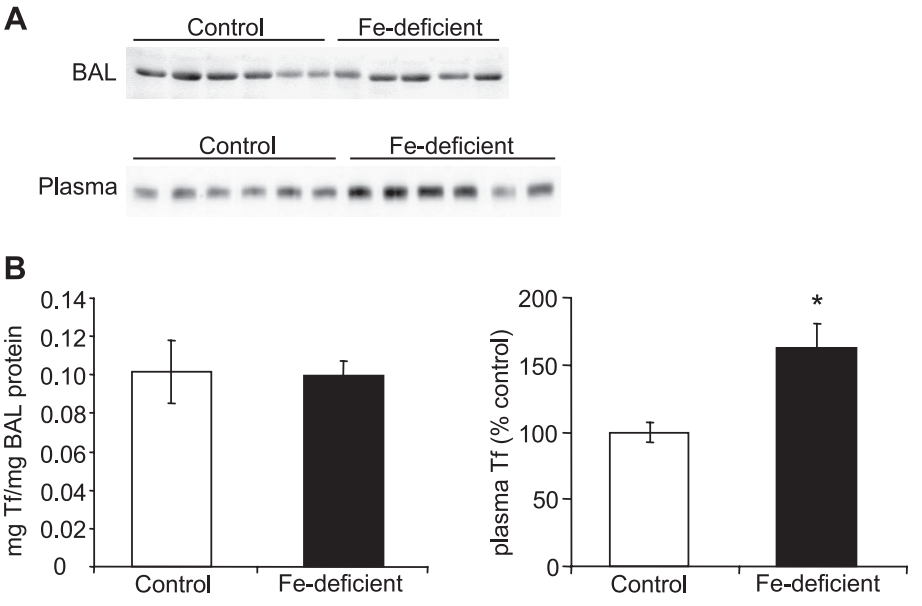

Fig. 3. Tf levels increase in plasma but not bronchoalveolar lavage (BAL) of iron-deficient rats. *A*: Western blot analysis was performed to determine Tf levels in BAL and plasma of control and Fe-deficient rats. *B*: band intensity detected by chemiluminescence was quantified using QuantityOne imaging software (Bio-Rad). *$P < 0.05$ ($n = 5$ to 6; means ± SE).

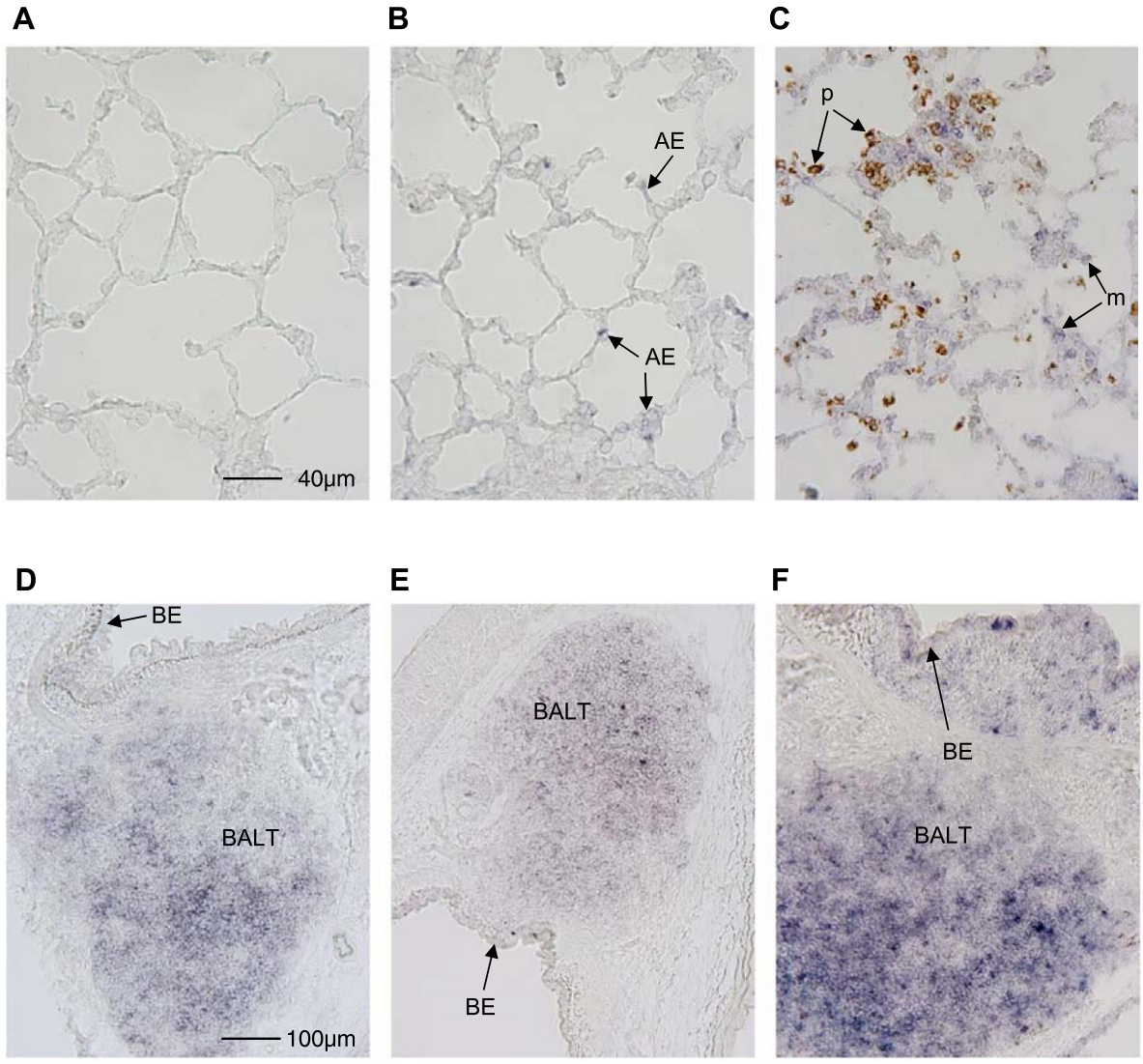

Fig. 4. In situ hybridization detecting lung TfR mRNA expression. In situ hybridization for TfR transcripts present in control (*A*, *D*), iron-deficient (*B*, *E*), and iron oxide-exposed (*C*, *F*) rat lungs was detected as described for Fig. 1. Magnification ×25 (*A–C*) and ×10 (*D–F*).

longer in vivo incubation periods (Fig. 5*C*). To demonstrate that ^{54}Mn bound to Tf would remain associated during fractionation, apoTf was loaded with ^{54}Mn in vitro and subjected to dialysis and anion exchange FPLC procedures. In vitro-radiolabeled ^{54}Mn-Tf was only detected in *fraction 17*, confirming that if present in BAL fluid, this species would be detected under our experimental conditions (Fig. 5*D*).

Table 1. *Distribution of ^{54}Mn and ^{59}Fe after intratracheal instillation*

	^{54}Mn, % Instilled Dose	^{59}Fe, % Instilled Dose
BAL (bound to protein)*	1.15±0.29	22.24±5.15
BAL (unbound)	13.40±3.20	5.29±1.62
BAL cell pellet	0.70±0.13	0.75±0.14
Lung tissue	55.01±3.38	54.08±8.17
Total in lungs	70.25±0.87	82.36±1.46

Values are means ± SE, $n = 3$. *Refers to radioactivity in bronchoalveolar lavage (BAL) after dialysis with molecular weight cutoff ≥ 14,000.

To identify the protein(s) that might bind ^{54}Mn in *fraction 15*, samples were pooled and concentrated. Six bands were detected by silver staining and identified by mass spectrometry (Fig. 6*B*). Of the proteins identified, only transketolase peaked in *fraction 15*. Transketolase is also the only protein identified in this fraction, other than Tf, that has been shown to bind manganese (30). Transketolase is a cytoplasmic enzyme that catalyzes transfer of dihydroxyethyl groups from ketose donors to aldose acceptors in the pentose phosphate pathway and is not predicted to function in ion transport (49).

Pharmacokinetics of ^{54}Mn absorption by Belgrade rats after intratracheal instillation. Because an association between instilled ^{54}Mn and Tf could not be detected in vivo, our findings suggested the possibility that soluble divalent manganese might be taken up directly by the lungs after instillation. One transporter that might be involved in pulmonary Mn^{2+} uptake is DMT1 (26, 56). Homozygous Belgrade (*b/b*) rats with defective DMT1 function exhibit reduced clearance of iron and vanadium from the lungs after instillation with ROFA com-

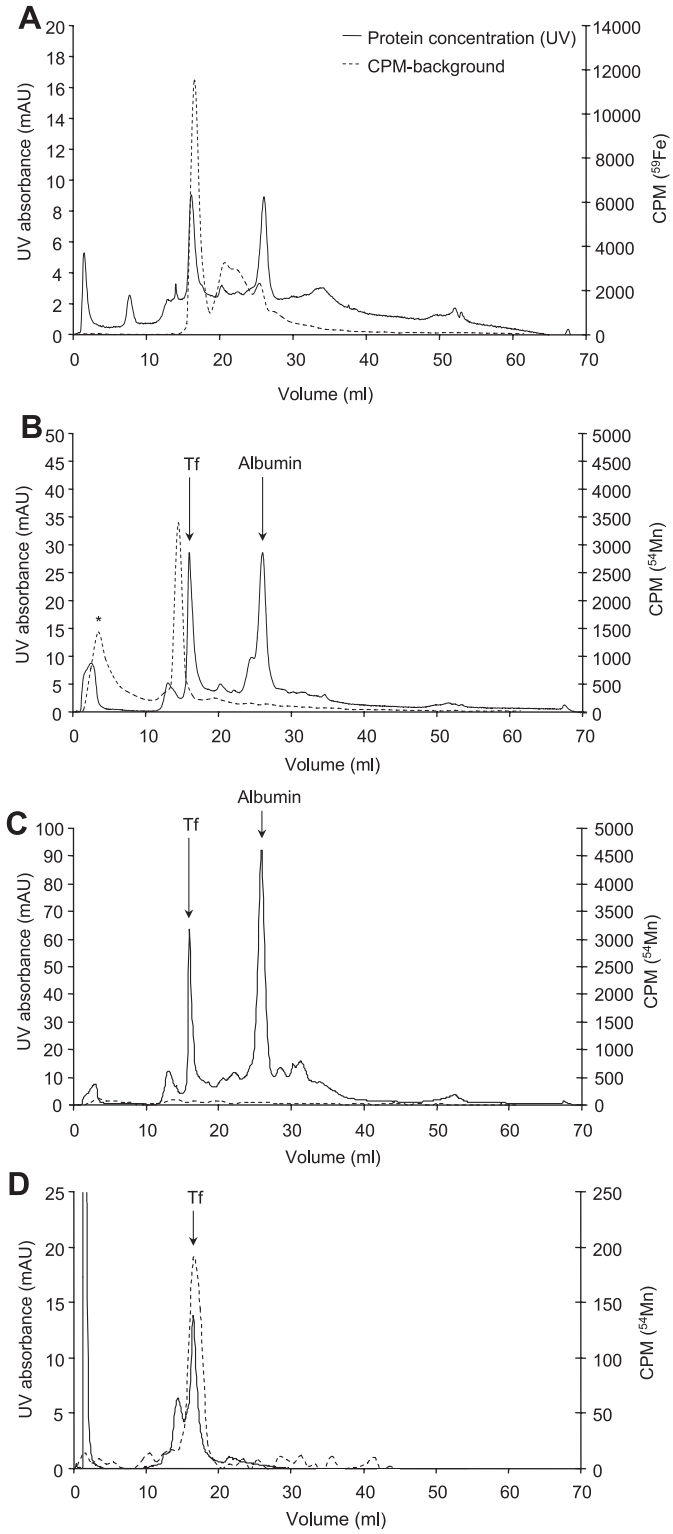

Fig. 5. Fast protein liquid chromatography (FPLC) fractionation of BAL. Lung fluid was collected by lavage 10 min after intratracheal instillation of ^{59}Fe (*A*) or ^{54}Mn (*B*), and 1 h after instillation of ^{54}Mn (*C*). Samples were dialyzed and proteins were fractionated by FPLC over an anion-exchange column as described under MATERIALS AND METHODS. To demonstrate detection of ^{54}Mn-Tf by this method, in vitro-labeled ^{54}Mn-Tf was also subjected to fractionation (*D*). Radioactivity in fractions was measured by gamma counting. The 2 major protein peaks in BAL were identified as transferrin and albumin (see Fig. 6). Solid line is trace of UV absorbance and dashed line shows cpm with background subtracted. AU, arbitrary units. *Flow-through fraction.

pared with heterozygous (*+/b*) controls (25). Therefore, we examined the pharmacokinetics of ^{54}Mn transport from the lungs to the blood after intratracheal instillation of homozygote (*b/b*) Belgrade rats and heterozygote (*+/b*) siblings. Figure 7 shows isotope levels determined in blood samples drawn from 5 min to 4 h postinstillation for both experimental groups. As previously observed (28), lung manganese absorption was quite rapid, with an initial drop in blood levels within 30 min postinstillation and relatively stable blood levels thereafter. The pharmacokinetics did not differ between *b/b* and *b/+* rats. At 4 h, circulating levels of ^{54}Mn in homozygous Belgrade and control heterozygous rats were similar (0.14 and 0.09%, respectively). The tissue distribution of ^{54}Mn determined 4 h postinstillation is shown in Table 2. The amounts of ^{54}Mn remaining in the lungs of *b/b* and *b/+* rats at this time point were also similar (60.73 and 64.09%, respectively), further indicating that pulmonary absorption of manganese was not impaired in Belgrade rats. The only differences noted in tissue distribution of ^{54}Mn after intratracheal instillation were that levels were significantly higher in the spleen and large intestine and lower in the kidneys of *b/b* rats compared with their littermate *b/+* controls (Table 2).

Characterization of ^{54}Mn uptake by A549 cells. To examine pathways for direct uptake of divalent manganese by the lungs, transport of $^{54}Mn^{2+}$ was characterized using A549 cells, a type II alveolar epithelial cell line. $^{54}Mn^{2+}$ uptake was time and temperature dependent (Fig. 8*A*). Uptake was also saturable with increasing Mn concentration (Fig. 8*B*). Uptake of $^{55}Fe^{2+}$ by A549 cells was increased at lower pH; however, $^{54}Mn^{2+}$ uptake at pH 6.75 was comparable to uptake observed at pH 7.4 (Fig. 9). These results suggest that DMT1 may be involved in ferrous iron uptake by alveolar epithelial cells as this membrane protein functions as a proton symporter, exhibiting increased Fe^{2+} and Mn^{2+} transport activity at pH 6.75 (22, 57). While the lack of a pH effect on A549 cell ^{54}Mn uptake does not rigorously rule out a possible role for DMT1 in transport of this metal in the lungs, it is in general agreement with the observations that uptake of intratracheally instilled ^{54}Mn is unimpaired in the Belgrade rat model.

Effect of calcium channel antagonists and agonists on ^{54}Mn uptake. We next examined whether Ca^{2+}, Fe^{2+}, or Ni^{2+} would compete with Mn for uptake by A549 cells (Fig. 10*A*). The observation that the presence of 500 μM Ca^{2+} inhibited uptake of ^{54}Mn suggested one or more calcium channels could be involved in the influx pathway. Coincubation with a 10- or 100-fold excess of Ni^{2+}, a broad-spectrum inhibitor of both voltage-gated and store-operated calcium channels, inhibited ^{54}Mn uptake by 69 and 86%, respectively. Likewise, dose-dependent inhibition by Fe^{2+} was observed with a 100-fold excess resulting in ~93% inhibition relative to uptake in control wells.

Pharmacological characteristics of various drugs with specificity for different Ca^{2+} channels suggested both voltage-gated channels (VGCs) and receptor-operated channels (ROCs), but not SOCs, are involved in manganese uptake by A549 cells (Fig. 10*B*). Treatment of cells with amiloride, an inhibitor with higher specificity for T-type VGCs, resulted in a relatively modest inhibition of transport (~10%). In contrast, the inhibitor verapamil, which acts on L-type VGCs, substantially reduced uptake and acted in a dose-dependent manner with ~65% inhibition at 500 μM. The dihydropyridine (DHP)

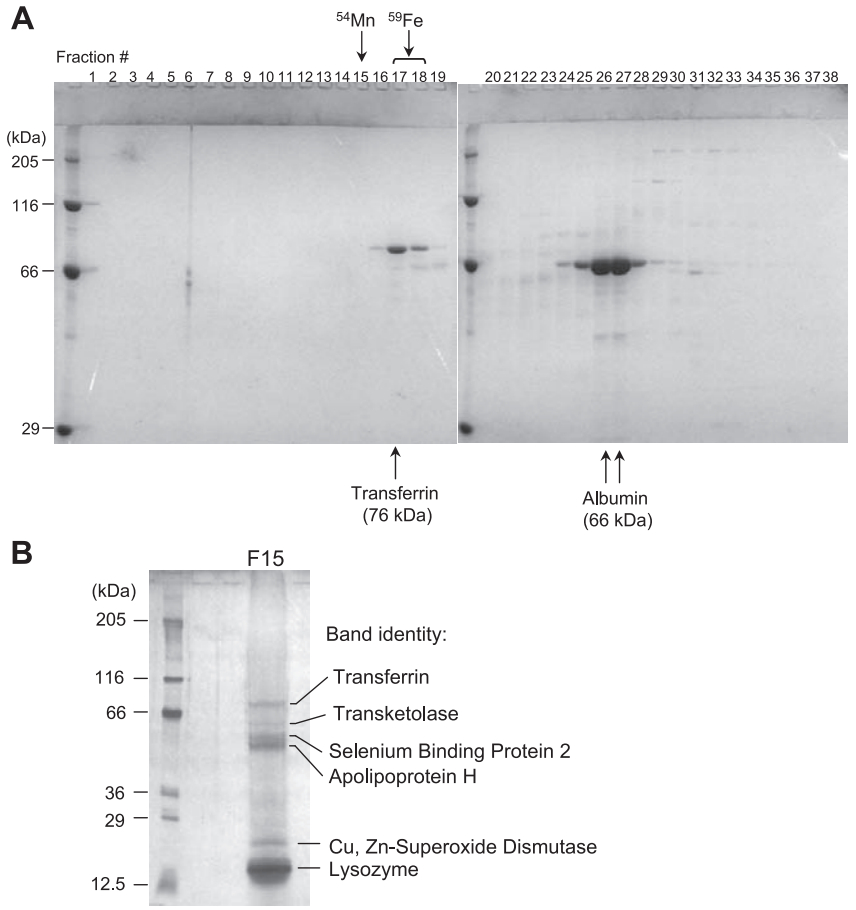

Fig. 6. Detection of proteins in BAL fluid. After anion-exchange FPLC chromatography, 1-ml fractions (as shown in Fig. 5) were concentrated. *A*: after electrophoresis on an 8% SDS-polyacrylamide gel, proteins were stained with Coomassie blue. *B*: proteins in *fraction 15* (*F15*) were concentrated, electrophoresed on a 5–20% gradient gel, and silver stained. Indicated bands were excised and identity of proteins was determined by mass spectrometry.

inhibitor nifedipine and the DHP activator *S*-(−)-BAY K 8644, which bind to a specific site on the α_1-subunit of L-type VGCs, had no effect on ^{54}Mn uptake. Thapsigargin, which causes release of Ca^{2+} from intracellular stores thereby activating SOCs, also had no effect. 2-APB, an inhibitor of the ROCs TRPC3, 6, and 7, reduced transport; however, the diacylglycerol analog OAG, which is reported to stimulate Ca^{2+} uptake by these members of the TRPC family (19, 29, 61), had no effect on ^{54}Mn uptake. Coincubation with 4 mM $MgCl_2$, which inhibits transport of divalent cations by TRPM7 (35), effectively decreased ^{54}Mn uptake by 75%.

Identification of TRP channels expressed by A549 cells. Electrophysiological studies in which Mn^{2+} was substituted for Ca^{2+} have demonstrated that several members of the TRPC (transient receptor potential canonical) subfamily are perme-

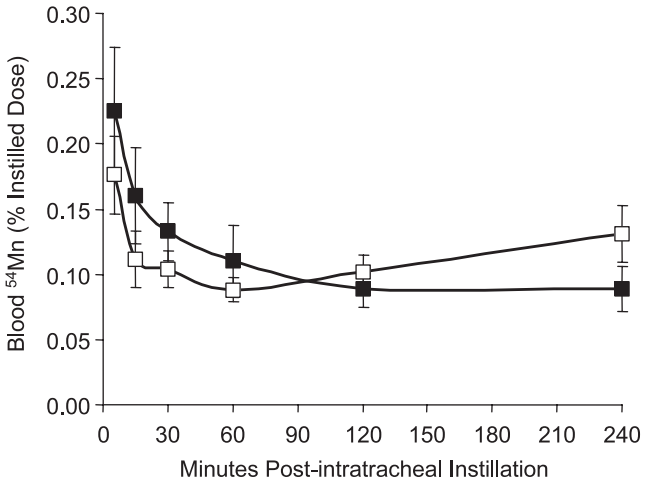

Fig. 7. Vascular kinetics of intratracheally instilled ^{54}Mn in Belgrade rats and heterozygous littermates. Heterozygous (*b*/+) rats (■) and Belgrade homozygous (*b*/*b*) rats (□) were administered ^{54}Mn by intratracheal instillation, and blood samples were drawn at the times indicated postinstillation. Blood ^{54}Mn levels are expressed as % of instilled dose. Each point is mean ± SE of 5 (*b*/*b*) or 7 (*b*/+) rats.

Table 2. *Tissue distribution of ^{54}Mn 4 h postinstillation*

	+/*b*	*b*/*b*
Brain	0.08±0.01	0.05±0.01
Liver	6.16±0.53	7.20±1.03
Spleen	0.15±0.02	0.45±0.06*
Lung	64.09±3.94	60.73±0.71
Kidney	1.84±0.19	1.26±0.11*
Heart	0.27±0.02	0.31±0.04
Bone marrow	0.59±0.05	0.54±0.04
Skeletal muscle	3.26±0.29	2.46±0.04
Esophagus	0.11±0.03	0.41±0.16
Stomach	0.85±0.22	0.96±0.22
Small intestine	3.13±0.45	2.93±0.54
Large intestine	6.48±1.01	9.78±1.71*
Total	87.76±4.36	87.21±3.30

Values (% instilled dose) are means ± SE (n = 5; MANOVA, *$P < 0.05$). +/*b*, Heterozygous rats; *b*/*b*, Belgrade homozygous rats.

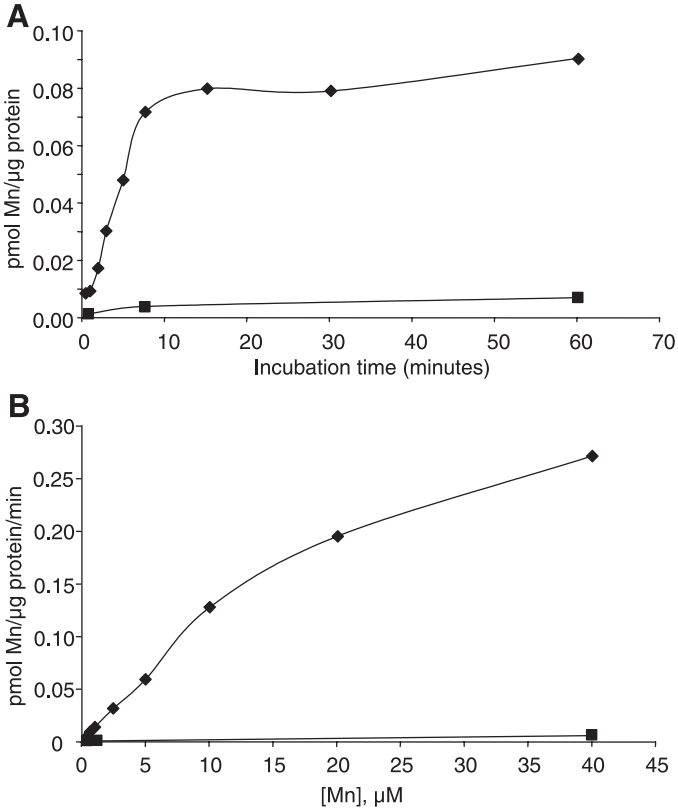

Fig. 8. Characteristics of ^{54}Mn uptake by A549 cells. A549 cells were grown to 70–80% confluency, washed with HeBS, incubated with 1–2 μCi ^{54}Mn at 4°C (squares) or 37°C (diamonds), and then incubated on ice for 1 h at 4°C to displace nonspecific binding of radioisotope. After being washed in HeBS, cells were lysed in solubilization buffer and the uptake was determined as pmol Mn/μg cell protein as described under MATERIALS AND METHODS. *A*: A549 cells were incubated with 0.68 μM $^{54}MnCl_2$ and the time course of uptake was determined. *B*: rate of $^{54}Mn^{2+}$ uptake was determined as a function of [Mn]. Assays similar to *A* were performed to measure uptake on incubation with the indicated concentrations of Mn for 4 min. The averages of duplicate determinations are shown.

able to manganese ions (9, 29). TRPM7, a member of the TRPM (melastatin) subfamily, is also permeable to several divalent metal ions, including Mn^{2+}. To determine which TRP channels are expressed by A549 cells, and to verify expression of LVGCs, RT-PCR was performed (Fig. 11). Expression of TRPC1, 3, 6, and 7, TRPM7, and the α_1-subunit of LVGC was detected. Interestingly, primers for TRPC7 amplified two products, one of the expected size (428 bp), and a smaller amplicon of ~200 bp. Because the 5′ and 3′ primers are located in different exons (exons 1 and 2, respectively), the 200-bp amplicon may be the result of alternative splicing of TRPC7 mRNA in A549 cells.

DISCUSSION

Manganism can result from inhalation of manganese-laden dust, making the lungs an important route of exposure to this potentially toxic metal. In this study, we investigated the molecular mechanisms of manganese uptake by pulmonary epithelial cells. Tf is reported to bind Mn in plasma (18) and is highly abundant in pulmonary fluid. In iron deficiency, circulating plasma Tf levels increase dramatically, and TfR expression is posttranscriptionally upregulated by iron regulatory protein (IRP) activation (11). Conversely, iron overload results in downregulation of TfR, coupled with increased expression of the cytosolic iron storage protein ferritin. Because Tf and TfR expression levels in the lungs could potentially affect clearance of inhaled metals, we examined expression of mRNA and protein in rats with iron deficiency and in rats exposed to iron oxide particles. In agreement with a previous report (60), our study shows that Tf mRNA is widely expressed by pulmonary cells, including bronchial epithelium, type II alveolar epithelial cells, macrophages, and focal regions of BALT (Fig. 1). Expression of Tf mRNA or protein in lung and BAL fluid did not change in iron deficiency, demonstrating that synthesis of Tf by pulmonary cells is regulated in response to the local environment of the lungs, rather than by systemic responses to iron status. Previous studies from our laboratory showed that iron deficiency does not enhance absorption of ^{59}Fe from the lungs and are consistent with these data (28). Iron oxide particles induced upregulation of Tf mRNA in bronchial and alveolar epithelium, macrophages, and BALT but protein levels did not change, although a nonsignificant trend toward increased Tf protein was detected in whole lung lysate.

TfR mRNA was detected primarily in BALT, with weak staining in bronchial epithelium. TfR mRNA expression was

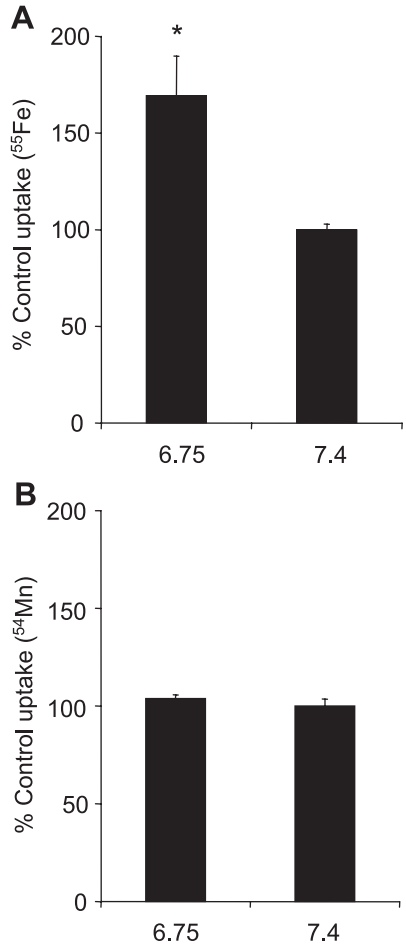

Fig. 9. pH dependence of ^{54}Mn and ^{55}Fe uptake by A549 cells. Cells were incubated with 1 μM ^{55}Fe (*A*) or ^{54}Mn (*B*) for 20 min in uptake buffer adjusted to pH 6.75 or 7.4 as described for Fig. 8 and in MATERIALS AND METHODS. *$P <$ 0.05 (n = 4; means ± SE).

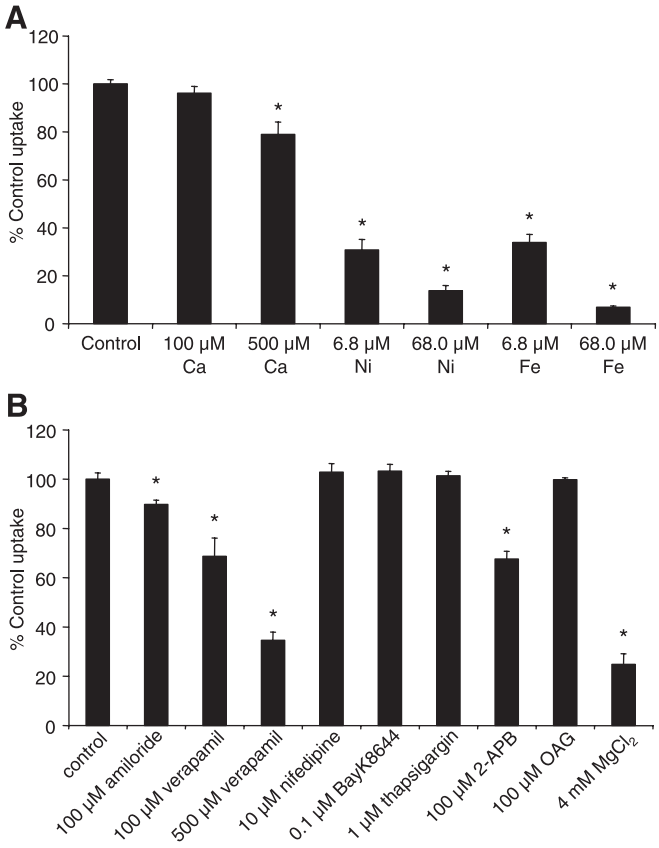

Fig. 10. Pharmacological profile of ^{54}Mn uptake by A549 cells. *A*: cells were incubated with 0.68 μM $^{54}Mn^{2+}$ in the presence or absence of other divalent cations at the concentrations indicated. *B*: transport assays with 0.34 μM $^{54}Mn^{2+}$ in the presence and absence of inhibitors/activators of L-type calcium channels, TRPC channels, and TRPM7. Cells were incubated with ^{54}Mn ± treatment or vehicle for 4 min. *$P < 0.05$ ($n = 3$–4; means ± SE).

enhanced in type II alveolar epithelial cells by iron deficiency, and TfR protein levels in whole lung were significantly increased. Iron oxide exposure also resulted in induction of TfR mRNA in lung; however, TfR protein levels did not change. Because ferritin was upregulated in iron oxide-exposed lung, it is unlikely that IRP activity accounts for posttranscriptional regulation of TfR mRNA. These findings suggest that while TfR gene expression may be induced at the transcriptional level by inflammatory stimuli (54), protein expression of lung TfR does not change when iron concentration is very high as a defense against cytotoxicity.

To test whether the Tf/TfR pathway might be involved in uptake of manganese, $^{54}Mn^{2+}$ was administered to rats by intratracheal instillation. At 10 min postinstillation, ~85% of the dose of ^{54}Mn had been absorbed from pulmonary fluid and only a small fraction (~1%) of the remaining ^{54}Mn was associated with BAL fluid protein. In contrast, 27% of the dose of intratracheally instilled $^{59}Fe^{2+}$ remained in BAL fluid, the majority of which was associated with Tf. These data suggest that while soluble $^{59}Fe^{2+}$ is oxidized to Fe^{3+} after instillation into the lungs and rapidly binds to Tf, $^{54}Mn^{2+}$ is directly taken up by pulmonary epithelial cells via Tf-independent pathways. This idea is confirmed by the fact that 1 h postinstillation, very little of the instilled ^{54}Mn remains bound to BAL fluid protein. It is likely that association of instilled soluble iron with Tf present in lung fluid is a first step in the process of pulmonary uptake of this metal and that this key difference contributes to the different pharmacokinetic profiles we previously observed for absorption of iron and manganese from the lungs to the blood (28). It should be noted that our experiments are limited to instillation studies of soluble forms of divalent ^{54}Mn and ^{59}Fe and that metals present in particulate matter inhaled into the lungs may be handled quite differently. For example, it is possible that trivalent manganese can associate with lung Tf after particle dissolution. Further investigation is necessary to test this idea.

Although DMT1 is known to play a role in the endocytic Tf/TfR pathway, the function of this divalent metal transporter at the plasma membrane could also provide a potential pathway for the direct uptake of Mn^{2+}. However, two separate lines of evidence argue against this possibility. In vivo experiments with Belgrade rats demonstrate that the impaired DMT1 activity of homozygous animals does not modify the pharmacokinetics of pulmonary ^{54}Mn absorption from the lungs to the blood. Moreover, in vitro studies of $^{54}Mn^{2+}$ uptake by A549 cells show that transport is not enhanced by low pH, indicating that DMT1 cannot be the predominant Mn transport activity. These results prompted us to consider alternative pathways for pulmonary manganese uptake. Pulmonary epithelial and endothelial cells express several calcium channels that are essential in maintenance of fluid balance in the lungs (34). Several recent publications have demonstrated that uptake of manganese into heart, liver, and brain is sensitive to modulators of LVGCs (12, 17, 52). Furthermore, patch-clamp studies have shown that several members of the TRPC subfamily of nonselective calcium channels are permeable to Mn^{2+} (9, 29). TRPC proteins are store-operated and/or receptor-operated calcium channels that can be activated by intracellular store depletion and/or by stimulation of G protein- or tyrosine kinase-coupled receptors (36). Formation of heteromultimeric complexes within subfamilies (e.g., TRPC4/5, TRPC3/6, TRPC1/3/7) produces channels with different characteristics and contributes to functional variability in vivo (48). Whether TRPC channels are permeable to Mn^{2+} in vivo is not clear. A

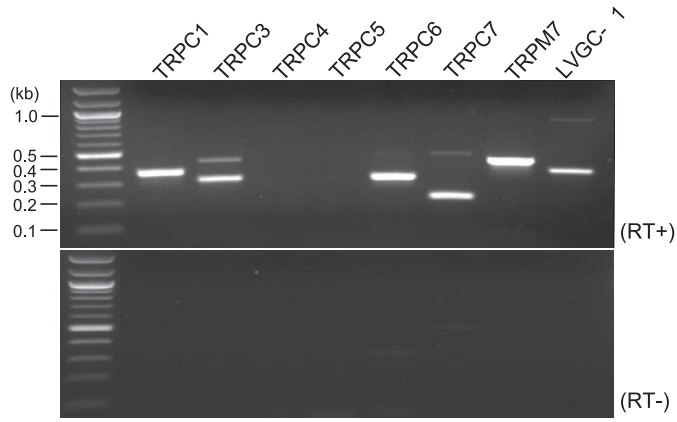

Fig. 11. Expression of transient receptor potential (TRP) channels and L-type voltage-gated calcium channel (LVGC) in A549 cells. To detect expression of indicated channels, reverse transcription-coupled PCR reactions were carried out with primers for TRPC1, 3, 6, and 7, TRPM7, and LVGC (α_1-subunit) as described under METHODS AND MATERIALS. *Top*: amplified products from A549 cDNA. *Bottom*: control reactions for which reverse transcriptase was omitted during cDNA synthesis.

widely expressed member of the TRP melastatin-related (TRPM) subfamily, TRPM7, is also implicated in Mn^{2+} transport. TRPM7 is important in cellular magnesium homeostasis and is involved in human disorders of magnesium metabolism (10). TRPM7 transports several divalent metal ions under physiological conditions, including Mn^{2+} (35, 37).

Analysis of gene expression of TRPC family members by RT-PCR and Northern blotting has shown that TRPC1, 3, 4, 5, 6, and 7, and TRPM7 are expressed in lung (43, 45). TRPC4 and 6 have been found in differentiated human bronchial epithelial cells, whereas TRPC3 and TRPM7 are expressed by bronchial epithelium-derived BEAS-2B cells (10, 13). Expression of TRPC1 and TRPC6 in A549 cells was previously reported (59). We have verified by RT-PCR that A549 cells express TRPC1, TRPC6, and LVGC and have additionally determined that TRPC3, TRPC7, and TRPM7 are also expressed in this cell line.

Pharmacological features of manganese transport in A549 cells were defined in our study by the effects of several calcium channel inhibitors and activators on $^{54}Mn^{2+}$ uptake. Treatment with verapamil, a phenylalkylamine antagonist that binds to the α_1-subunit of LVGC, caused a significant dose-responsive reduction in ^{54}Mn uptake. Treatment with the DHP antagonist nifedipine or the activator BAY K 8644, both of which bind to a specific site on the α_1-subunit distinct from the binding site of verapamil, did not have an effect. Because the efficacy of DHP drugs appears to be voltage dependent, their lack of effect in A549 cells could be due to the fact that these cells are at resting potential (4, 47). Alternatively, verapamil could potentially inhibit Mn influx through TRPC3 (63) or by another uncharacterized mechanism.

To determine whether manganese influx might also occur through SOCs, including TRPC1 and TRPC7 (31), A549 cells were treated with thapsigargin, an inhibitor of sarcoplasmic/endoplasmic reticulum Ca^{2+} ATPase that produces a rapid increase in cytosolic [Ca], triggering opening of SOCs on the plasma membrane. Treatment with thapsigargin has previously been shown to increase Ca^{2+} influx and trigger Mn^{2+}-mediated quenching of fura-2 fluorescence in A549 cells (59). We did not observe any effect of thapsigargin on ^{54}Mn uptake, but we note that the concentration of Mn^{2+} studied by Xue et al. (59) was 1.2 mM, ~2,000-fold greater than the concentrations used in our assays.

2-APB is a noncompetitive inhibitor of the IP_3 receptor which blocks activation of ROCs in response to G protein-coupled receptor (GPCR)-mediated phospholipase C (PLC) activation (32). 2-APB can also act directly on TRPC3, TRPC5, TRPC6, and TRPC7, possibly by binding in the pore region of these channels (31, 58). Inhibition of ^{54}Mn uptake by 2-APB suggests involvement of one or more of the 2-APB-sensitive TRPC proteins that behave as ROCs. However, we found that OAG, a membrane-permeable diacylglycerol (DAG) analog that activates TRPC3, 6, and 7, had no effect on ^{54}Mn uptake. The subunit composition of TRPC heteromeric channels in vivo modulates sensitivity to DAG (50) and could explain this apparently contradictory finding. A second explanation might be that TRPM7 is responsible for manganese uptake. One report has indicated that calcium influx through TRPM7 is also sensitive to 2-APB treatment (27). Unlike the TRPC channels, TRPM7 is inhibited by PLC-mediated depletion of PIP_2 following GPCR stimulation and is not activated by OAG (1, 46). Depletion of intracellular Mg^{2+} and Mg-ATP activates TRPM7, and high concentrations of either form of magnesium inhibit channel activity (38). In our assays, addition of 4 mM $MgCl_2$ resulted in a 75% inhibition of $^{54}Mn^{2+}$ uptake by A549 cells, supporting a key role for this channel. The preference of TRPM7 for manganese and other divalent metals over calcium make this channel a plausible candidate for manganese transport in vivo (35).

In conclusion, transition metals in ambient particulate matter from diesel exhaust, ROFA, and coal dust are thought to be the component(s) responsible for increased airway hyperresponsiveness, inflammation, and oxidative stress from these exposures (23, 42). We have characterized changes in Tf and TfR expression in the lungs in response to iron status that may reflect how the lungs handle metal burden to minimize oxidative damage. Of equal importance are the mechanisms by which potentially toxic inhaled metals enter the blood stream. While a role for lung fluid Tf in iron absorption should be tested more rigorously, our results suggest that ferrous iron can be readily oxidized to bind Tf and that elements of the Tf/TfR/DMT1 pathway may mediate its absorption from the lungs. In contrast, our instillation studies indicate that soluble Mn^{2+} does not interact with Tf in BAL fluid, suggesting alternative pathways for uptake are responsible for its transport from the lungs. One caveat is that the potential role for the Tf/TfR/DMT1 pathway in the uptake of trivalent Mn cannot be rigorously ruled out as it is possible that on dissolution, metal from particulate matter could be oxidized and cleared by this pathway. Our findings do support a potential role for TRPM7, LVGCs, and possibly other TRP channels in the process of lung Mn^{2+} absorption. It will be of great interest to determine whether such channels function in transport of trace metals in the lungs in vivo and whether exposure to components of particulate matter and/or resulting inflammation might affect channel activity.

ACKNOWLEDGMENTS

We thank T. Donaghey and K. Doud for excellent technical help.

GRANTS

This work was supported by National Institutes of Health Grant DK-60528 to M. Wessling-Resnick and grants from the American Welding Society to J. D. Brain. Support for proteomic analysis was provided by the Harvard School of Public Health-National Institute of Environmental Health Sciences (NIEHS) Center for Environmental Health (ES-00002). Additional support for the interpretation of results and authorship of this publication was made possible by Grant P01-ES-012874 from NIEHS and from STAR Research Assistance Agreement No. RD-83172501 awarded by the US Environmental Protection Agency (EPA).

DISCLOSURES

This work has not been formally reviewed by either the NIEHS or EPA. The views expressed in this document are solely those of the authors and do not necessarily reflect those of either the NIEHS or the EPA. Neither NIEHS nor the EPA endorses any products or commercial services mentioned in this publication.

REFERENCES

1. **Aarts M, Iihara K, Wei WL, Xiong ZG, Arundine M, Cerwinski W, MacDonald JF, and Tymianski M.** A key role for TRPM7 channels in anoxic neuronal death. *Cell* 115: 863–877, 2003.
2. **Aisen P, Aasa R, and Redfield AG.** The chromium, manganese, and cobalt complexes of transferrin. *J Biol Chem* 244: 4628–4633, 1969.

3. **ATSDR.** *Toxicological Profile for Manganese*. Atlanta, GA: US Dept. of Health and Human Services, Public Health Service, Agency for Toxic Substances and Disease Registry, prepared by Research Triangle Institute, 2000.
4. **Bean BP.** Nitrendipine block of cardiac calcium channels: high-affinity binding to the inactivated state. *Proc Natl Acad Sci USA* 81: 6388–6392, 1984.
5. **Bothwell TH, Charlton RW, Cook JD, and Finch CA.** *Iron Metabolism in Man*. Oxford, UK: Blackwell Scientific Publications, 1979.
6. **Bradford MM.** A rapid and sensitive method for the quantitation of microgram quantities of protein utilizing the principle of protein-dye binding. *Anal Biochem* 72: 248–254, 1976.
7. **Brain JD, Heilig EA, Donaghey TC, Knutson MD, Wessling-Resnick M, and Molina RM.** Effects of iron status on transpulmonsry transport and tissue distribution of Mn and Fe. *Am J Respir Cell Mol Biol* In press.
8. **Brain JD, Knudson DE, Sorokin SP, and Davis MA.** Pulmonary distribution of particles given by intratracheal instillation or by aerosol inhalation. *Environ Res* 11: 13–33, 1976.
9. **Chen J and Barritt GJ.** Evidence that TRPC1 (transient receptor potential canonical 1) forms a Ca^{2+}-permeable channel linked to the regulation of cell volume in liver cells obtained using small interfering RNA targeted against TRPC1. *Biochem J* 373: 327–336, 2003.
10. **Chubanov V, Waldegger S, Mederos y Schnitzler M, Vitzthum H, Sassen MC, Seyberth HW, Konrad M, and Gudermann T.** Disruption of TRPM6/TRPM7 complex formation by a mutation in the TRPM6 gene causes hypomagnesemia with secondary hypocalcemia. *Proc Natl Acad Sci USA* 101: 2894–2899, 2004.
11. **Chung J and Wessling-Resnick M.** Molecular mechanisms and regulation of iron transport. *Crit Rev Clin Lab Sci* 40: 151–182, 2003.
12. **Colet JM, Vander Elst L, and Muller RN.** Dynamic evaluation of the hepatic uptake and clearance of manganese-based MRI contrast agents: a 31P NMR study on the isolated and perfused rat liver. *J Magn Reson Imaging* 8: 663–669, 1998.
13. **Corteling RL, Li S, Giddings J, Westwick J, Poll C, and Hall IP.** Expression of transient receptor potential C6 and related transient receptor potential family members in human airway smooth muscle and lung tissue. *Am J Respir Cell Mol Biol* 30: 145–154, 2004.
14. **Costa DL and Dreher KL.** Bioavailable transition metals in particulate matter mediate cardiopulmonary injury in healthy and compromised animal models. *Environ Health Perspect* 105, *Suppl* 5: 1053–1060, 1997.
15. **Cotzias GC, Horiuchi K, Fuenzalida S, and Mena I.** Chronic manganese poisoning. Clearance of tissue manganese concentrations with persistance of the neurological picture. *Neurology* 18: 376–382, 1968.
16. **Crossgrove JS, Allen DD, Bukaveckas BL, Rhineheimer SS, and Yokel RA.** Manganese distribution across the blood-brain barrier. I. Evidence for carrier-mediated influx of managanese citrate as well as manganese and manganese transferrin. *Neurotoxicology* 24: 3–13, 2003.
17. **Crossgrove JS and Yokel RA.** Manganese distribution across the blood-brain barrier. IV. Evidence for brain influx through store-operated calcium channels. *Neurotoxicology* 26: 297–307, 2005.
18. **Davidsson L, Lonnerdal B, Sandstrom B, Kunz C, and Keen CL.** Identification of transferrin as the major plasma carrier protein for manganese introduced orally or intravenously or after in vitro addition in the rat. *J Nutr* 119: 1461–1464, 1989.
19. **Dietrich A, Kalwa H, Rost BR, and Gudermann T.** The diacylglycerol-sensitive TRPC3/6/7 subfamily of cation channels: functional characterization and physiological relevance. *Pflügers Arch* 451: 72–80, 2005.
20. **Dorman DC, Struve MF, Gross EA, Wong BA, and Howroyd PC.** Subchronic inhalation of high concentrations of manganese sulfate induces lower airway pathology in rhesus monkeys. *Respir Res* 6: 121, 2005.
21. **Fleming MD, Romano MA, Su MA, Garrick LM, Garrick MD, and Andrews NC.** Nramp2 is mutated in the anemic Belgrade (b) rat: evidence of a role for Nramp2 in endosomal iron transport. *Proc Natl Acad Sci USA* 95: 1148–1153, 1998.
22. **Forbes JR and Gros P.** Iron, manganese, and cobalt transport by Nramp1 (Slc11a1) and Nramp2 (Slc11a2) expressed at the plasma membrane. *Blood* 102: 1884–1892, 2003.
23. **Gavett SH and Koren HS.** The role of particulate matter in exacerbation of atopic asthma. *Int Arch Allergy Immunol* 124: 109–112, 2001.
24. **Ghio AJ, Carter JD, Samet JM, Reed W, Quay J, Dailey LA, Richards JH, and Devlin RB.** Metal-dependent expression of ferritin and lactoferrin by respiratory epithelial cells. *Am J Physiol Lung Cell Mol Physiol* 274: L728–L736, 1998.
25. **Ghio AJ, Piantadosi CA, Wang X, Dailey LA, Stonehuerner JD, Madden MC, Yang F, Dolan KG, Garrick MD, and Garrick LM.** Divalent metal transporter-1 decreases metal-related injury in the lung. *Am J Physiol Lung Cell Mol Physiol* 289: L460–L467, 2005.
26. **Gunshin H, Mackenzie B, Berger UV, Gunshin Y, Romero MF, Boron WF, Nussberger S, Gollan JL, and Hediger MA.** Cloning and characterization of a mammalian proton-coupled metal-ion transporter. *Nature* 388: 482–488, 1997.
27. **Hanano T, Hara Y, Shi J, Morita H, Umebayashi C, Mori E, Sumimoto H, Ito Y, Mori Y, and Inoue R.** Involvement of TRPM7 in cell growth as a spontaneously activated Ca^{2+} entry pathway in human retinoblastoma cells. *J Pharm Sci* 95: 403–419, 2004.
28. **Heilig E, Molina R, Donaghey T, Brain JD, and Wessling-Resnick M.** Pharmacokinetics of pulmonary manganese absorption: evidence for increased susceptibility to manganese loading in iron-deficient rats. *Am J Physiol Lung Cell Mol Physiol* 288: L887–L893, 2005.
29. **Hofmann T, Obukhov AG, Schaefer M, Harteneck C, Gudermann T, and Schultz G.** Direct activation of human TRPC6 and TRPC3 channels by diacylglycerol. *Nature* 397: 259–263, 1999.
30. **Jung EH, Takeuchi T, Nishino K, and Itokawa Y.** Studies on the nature of thiamine pyrophosphate binding and dependency on divalent cations of transketolase from human erythrocytes. *Int J Biochem* 20: 1255–1259, 1988.
31. **Lievremont JP, Bird GS, and Putney JW Jr.** Canonical transient receptor potential TRPC7 can function as both a receptor- and store-operated channel in HEK-293 cells. *Am J Physiol Cell Physiol* 287: C1709–C1716, 2004.
32. **Maruyama T, Kanaji T, Nakade S, Kanno T, and Mikoshiba K.** 2APB, 2-aminoethoxydiphenyl borate, a membrane-penetrable modulator of Ins(1,4,5)P3-induced Ca^{2+} release. *J Biochem (Tokyo)* 122: 498–505, 1997.
33. **Masumiya H, Tsujikawa H, Hino N, and Ochi R.** Modulation of manganese currents by 1,4-dihydropyridines, isoproterenol and forskolin in rabbit ventricular cells. *Pflügers Arch* 446: 695–701, 2003.
34. **Mehta D, Bhattacharya J, Matthay MA, and Malik AB.** Integrated control of lung fluid balance. *Am J Physiol Lung Cell Mol Physiol* 287: L1081–L1090, 2004.
35. **Monteilh-Zoller MK, Hermosura MC, Nadler MJ, Scharenberg AM, Penner R, and Fleig A.** TRPM7 provides an ion channel mechanism for cellular entry of trace metal ions. *J Gen Physiol* 121: 49–60, 2003.
36. **Montell C.** The TRP superfamily of cation channels. *Sci STKE 2005*: re3, 2005.
37. **Mwanjewe J and Grover AK.** Role of transient receptor potential canonical 6 (TRPC6) in non-transferrin-bound iron uptake in neuronal phenotype PC12 cells. *Biochem J* 378: 975–982, 2004.
38. **Nadler MJ, Hermosura MC, Inabe K, Perraud AL, Zhu Q, Stokes AJ, Kurosaki T, Kinet JP, Penner R, Scharenberg AM, and Fleig A.** LTRPC7 is a Mg.ATP-regulated divalent cation channel required for cell viability. *Nature* 411: 590–595, 2001.
39. **Pacht ER and Davis WB.** Role of transferrin and ceruloplasmin in antioxidant activity of lung epithelial lining fluid. *J Appl Physiol* 64: 2092–2099, 1988.
40. **Peng J, Elias JE, Thoreen CC, Licklider LJ, and Gygi SP.** Evaluation of multidimensional chromatography coupled with tandem mass spectrometry (LC/LC-MS/MS) for large-scale protein analysis: the yeast proteome. *J Proteome Res* 2: 43–50, 2003.
41. **Prahalad AK, Soukup JM, Inmon J, Willis R, Ghio AJ, Becker S, and Gallagher JE.** Ambient air particles: effects on cellular oxidant radical generation in relation to particulate elemental chemistry. *Toxicol Appl Pharmacol* 158: 81–91, 1999.
42. **Quinlan GJ, Evans TW, and Gutteridge JM.** Iron and the redox status of the lungs. *Free Radic Biol Med* 33: 1306–1313, 2002.
43. **Riccio A, Medhurst AD, Mattei C, Kelsell RE, Calver AR, Randall AD, Benham CD, and Pangalos MN.** mRNA distribution analysis of human TRPC family in CNS and peripheral tissues. *Brain Res Mol Brain Res* 109: 95–104, 2002.
44. **Roels H, Lauwerys R, Buchet JP, Genet P, Sarhan MJ, Hanotiau I, de Fays M, Bernard A, and Stanescu D.** Epidemiological survey among workers exposed to manganese: effects on lung, central nervous system, and some biological indices. *Am J Ind Med* 11: 307–327, 1987.
45. **Runnels LW, Yue L, and Clapham DE.** TRP-PLIK, a bifunctional protein with kinase and ion channel activities. *Science* 291: 1043–1047, 2001.

46. **Runnels LW, Yue L, and Clapham DE.** The TRPM7 channel is inactivated by PIP(2) hydrolysis. *Nat Cell Biol* 4: 329–336, 2002.
47. **Sanguinetti MC and Kass RS.** Voltage-dependent block of calcium channel current in the calf cardiac Purkinje fiber by dihydropyridine calcium channel antagonists. *Circ Res* 55: 336–348, 1984.
48. **Schaefer M.** Homo- and heteromeric assembly of TRP channel subunits. *Pflügers Arch* 451: 35–42, 2005.
49. **Schenk G, Duggleby RG, and Nixon PF.** Properties and functions of the thiamin diphosphate dependent enzyme transketolase. *Int J Biochem Cell Biol* 30: 1297–1318, 1998.
50. **Strubing C, Krapivinsky G, Krapivinsky L, and Clapham DE.** Formation of novel TRPC channels by complex subunit interactions in embryonic brain. *J Biol Chem* 278: 39014–39019, 2003.
51. **Thompson AB, Bohling T, Payvandi F, and Rennard SI.** Lower respiratory tract lactoferrin and lysozyme arise primarily in the airways and are elevated in association with chronic bronchitis. *J Lab Clin Med* 115: 148–158, 1990.
52. **Tsushima RG, Wickenden AD, Bouchard RA, Oudit GY, Liu PP, and Backx PH.** Modulation of iron uptake in heart by L-type Ca^{2+} channel modifiers: possible implications in iron overload. *Circ Res* 84: 1302–1309, 1999.
53. **Tu CL, Chang W, and Bikle DD.** Phospholipase cγ1 is required for activation of store-operated channels in human keratinocytes. *J Invest Dermatol* 124: 187–197, 2005.
54. **Upton RL, Chen Y, Mumby S, Gutteridge JM, Anning PB, Nicholson AG, Evans TW, and Quinlan GJ.** Variable tissue expression of transferrin receptors: relevance to acute respiratory distress syndrome. *Eur Respir J* 22: 335–341, 2003.
55. **Valberg PA and Brain JD.** Generation and use of three types of iron-oxide aerosol. *Am Rev Respir Dis* 120: 1013–1024, 1979.
56. **Wang X, Ghio AJ, Yang F, Dolan KG, Garrick MD, and Piantadosi CA.** Iron uptake and Nramp2/DMT1/DCT1 in human bronchial epithelial cells. *Am J Physiol Lung Cell Mol Physiol* 282: L987–L995, 2002.
57. **Worthington MT, Browne L, Battle EH, and Luo RQ.** Functional properties of transfected human DMT1 iron transporter. *Am J Physiol Gastrointest Liver Physiol* 279: G1265–G1273, 2000.
58. **Xu SZ, Zeng F, Boulay G, Grimm C, Harteneck C, and Beech DJ.** Block of TRPC5 channels by 2-aminoethoxydiphenyl borate: a differential, extracellular and voltage-dependent effect. *Br J Pharmacol* 145: 405–414, 2005.
59. **Xue HH, Zhao DM, Suda T, Uchida C, Oda T, Chida K, Ichiyama A, and Nakamura H.** Store depletion by caffeine/ryanodine activates capacitative Ca^{2+} entry in nonexcitable A549 cells. *J Biochem (Tokyo)* 128: 329–336, 2000.
60. **Yang F, Friedrichs WE, and Coalson JJ.** Regulation of transferrin gene expression during lung development and injury. *Am J Physiol Lung Cell Mol Physiol* 273: L417–L426, 1997.
61. **Zagranichnaya TK, Wu X, and Villereal ML.** Endogenous TRPC1, TRPC3, and TRPC7 proteins combine to form native store-operated channels in HEK-293 cells. *J Biol Chem* 280: 29559–29569, 2005.
62. **Zayed J.** Use of MMT in Canadian gasoline: health and environment issues. *Am J Ind Med* 39: 426–433, 2001.
63. **Zhu X, Jiang M, and Birnbaumer L.** Receptor-activated Ca^{2+} influx via human Trp3 stably expressed in human embryonic kidney (HEK)293 cells. Evidence for a non-capacitative Ca^{2+} entry. *J Biol Chem* 273: 133–142, 1998.